UNIVERSITAT DE BARCELONA

Superfluid fraction in disordered bosonic gases

Author:
Daniel Pérez Cruz

Supervisors:
Pietro Massignan and Grigori Astrakharchik

A MASTER THESIS FOR

MASTER IN QUANTUM SCIENCE AND TECHNOLOGY

University of Barcelona, July 2023

Superfluid fraction in disordered bosonic gases

Daniel Pérez Cruz

Supervised by: Pietro Massignan and Grigori Astrakharchik

Barcelona Quantum Monte Carlo group, Universitat Politècnica de Catalunya, 08034 Barcelona

14th July 2023

In this work, we study the behaviour of the superfluid fraction f of a bosonic system under the influence of a speckle potential. We start by introducing and defining f, and then we present the lower and upper bounds to f derived by A. Leggett for generic many-body systems. To benchmark our codes, we study first the case of a periodic optical potential, reproducing results that recently appeared in the literature. We continue by describing the particular kind of disordered potential we want to study, and how this is characterized. Finally, we compute the superfluid fraction as a function of the intensity of the disordered potential and the interaction strength between the bosons, and we compare our results to the two bounds in both 1D and 2D.

Keywords: Gross-Pitaevskii equation, superfluid fraction, Leggett's bounds, disordered (speckle) potentials

Acknowledgements

I am deeply grateful for all the help and advice that Pietro has provided me with during these past months. His profound knowledge of physics and, especially, his kindness have transformed this work into a quite wonderful experience. I cannot thank him enough for all the effort and time he has dedicated to teaching me the intricacies of physics.

I would also like to thank Grigori for his insight and comments. His great physical intuition always pointed us in the right direction and helped us overcome every complication that we found along the way.

Finally, to my family. Not only for letting me pursue my dreams but also for teaching me how to do so.

Contents

1 Basics of the Gross-Pitaevskii theory **2**

1.1 Relevant energies and length scales 3

2 Superfluid fraction in Bose-Einstein condensates **4**

Daniel Pérez Cruz: dapecr13@gmail.com

2.1 Dynamical effects of superfluidity . . . 4
2.2 Leggett's bounds . . . 6

3 Superfluid fraction in an optical lattice **7**

4 Disordered potentials **9**
4.1 Speckle potentials . . . 9
4.2 Statistical properties of the speckle potential . . . 10
4.3 Self-averaging property . . . 11

5 Superfluid fraction in a one-dimensional speckle potential **11**

6 Superfluid fraction in two-dimensional speckle potentials **13**
6.1 Choice of the wavefunction . . . 14
6.2 Localization process in a two-dimensional speckle potential . . . 14
6.3 Finite size effects . . . 15

7 Conclusions **16**

8 Outlook **17**

A Numerical solution of the GPE **18**
A.1 Imaginary time evolution . . . 19

B Strang splitting **20**

Bibliography **22**

1 Basics of the Gross-Pitaevskii theory

The many-body problem in classical physics is well known to quickly become intractable by analytical means. The same happens in the quantum regime, where we are interested in modelling the following system:

$$\mathbf{H} = \sum_{i=1}^{N} \left[\frac{\hat{\mathbf{P}}_i^2}{2m} + V_{\text{ext}}(\mathbf{r}_i) \right] + \sum_{i<j} V(\mathbf{r}_i - \mathbf{r}_j). \tag{1}$$

This Hamiltonian describes a gas of N quantum particles with mass m in an external potential $V_{\text{ext}}(\mathbf{r}_i)$ interacting through a pair potential $V(\mathbf{r}_i - \mathbf{r}_j)$. In the low-energy regime, the pair potential can be approximated by a contact interaction whose strength is given by a coupling parameter that we call g. It gives us a measure of the strength of the interactions, and is related to the three-dimensional s-wave scattering length a_s through:

$$g = \frac{4\pi\hbar^2 a_s}{m}.$$

Even though it is already an approximation, solving Eq. (1) is a formidable task. Instead of doing so, we use a mean-field approach to tackle the problem. Here, we partially reproduce some key steps of the derivation of the so-called Gross-Pitaevskii equation to understand the assumptions that are behind the theory.

In a dilute Bose gas at very low temperatures, all bosons occupy the same single-particle normalized state, so the multiparticle wavefunction reads:

$$\Psi(\{\mathbf{r}\}) = \prod_i \phi(\mathbf{r}_i).$$

Computing the energy of this state we find [PS08]:

$$E = N \int d\mathbf{r} \left[\frac{\hbar^2}{2m} |\nabla\phi|^2 + V(\mathbf{r})|\phi(\mathbf{r})|^2 + g\frac{N-1}{2}|\phi(\mathbf{r})|^4 \right].$$

Defining the so-called condensate wavefunction as:

$$\psi(\mathbf{r}) = \sqrt{N}\phi(\mathbf{r}) \qquad \left(\int d\mathbf{r}|\psi|^2 = N \right),$$

and using the fact that N is large, we can rewrite the energy as:

$$E = \int d\mathbf{r} \left[-\frac{\hbar^2}{2m}\nabla^2\psi(\mathbf{r}) + V(\mathbf{r})|\psi(\mathbf{r})|^2 + \frac{g}{2}|\psi(\mathbf{r})|^4 \right]. \tag{2}$$

The next step is to find the optimal form for ψ. This may be done by minimizing the free energy $E - \mu N$ for fixed chemical potential μ. Following this procedure, one finds the time-independent Gross-Pitaevskii equation (GPE from now on):

$$-\frac{\hbar^2}{2m}\nabla^2\psi(\mathbf{r}) + V(\mathbf{r})\psi(\mathbf{r}) + g|\psi(\mathbf{r})|^2\psi(\mathbf{r}) = \mu\psi(\mathbf{r}). \tag{3}$$

Let us briefly review the conditions of applicability of this equation:

- We are neglecting any interaction between degrees of freedom whose characteristic length scale is smaller than the average interparticle distance. Their effects are incorporated in the description through the contact interaction.
- It is necessary that the scattering length is much smaller than the average interparticle distance ($n_0^{1/3}, n_0 = N/L^3$). This means that the so-called **gas parameter** must fulfil: $n_0^{1/3}a_s \ll 1$. This condition must be met to have a well-defined mean-field picture. Under these conditions, the depletion of the condensate, which goes as $\sqrt{n_0 a_s^3}$, is negligible.
- Quantum fluctuations are not captured in this approach, so the mean-field theory does not give correct results near phase transitions or in strongly interacting systems.

1.1 Relevant energies and length scales

Here we present some important magnitudes that allow us to characterize Bose-Einstein condensates. The first one is the so-called chemical potential, that has already appeared in the previous section as a Lagrange multiplier. We can compute it as:

$$\mu = \int d\mathbf{r} \left[-\frac{\hbar^2}{2m}\nabla^2\psi(\mathbf{r}) + V(\mathbf{r})|\psi(\mathbf{r})|^2 + g|\psi(\mathbf{r})|^4 \right]. \tag{4}$$

So we see that the relation between energy and chemical potential is:

$$E = \mu - \frac{g}{2}\int d\mathbf{r}|\psi(\mathbf{r})|^4.$$

The chemical potential plays a role similar to that of the energy in the non-interacting case, in the sense that it gives a measure of the capacity of the condensate to penetrate potential barriers. Strictly speaking, the chemical potential gives us the energy gained or released by the system when a particle is added or removed. The chemical potential for a uniform Bose gas reduces to $\mu_0 = gn_0$.

The next relevant quantity is the so-called healing length of the condensate. It gives us a measure of the minimum length scale over which the condensate wavefunction changes. It is a property of the BEC and completely independent of the external potential. It can be obtained by finding the length at which the kinetic energy equals the interaction energy. Calling ξ this natural length scale, the kinetic energy and the interaction term are roughly equal when:

$$\frac{\hbar^2}{2m\xi^2} = gn_0 = \mu_0,$$

so that the healing length turns out to be:

$$\xi = \sqrt{\frac{\hbar^2}{2mgn_0}} = \sqrt{\frac{\hbar^2}{2m\mu_0}}. \tag{5}$$

2 Superfluid fraction in Bose-Einstein condensates

2.1 Dynamical effects of superfluidity

When describing the state of a Bose-Einstein gas, a quite useful description is that of the two-fluid model. A Bose-Einstein condensate, at sufficiently low temperature, can have a fraction of its components in the so-called superfluid state, while the remaining fraction of the system is referred to as the normal component, associated with excitations.

A superfluid exhibits a series of counter-intuitive properties that are extremely related to those of superconductors. A couple of these properties are the non-classical responses to external perturbations or the capacity to flow without losses. In experiments, one can generally test only the whole system (superfluid plus normal component), therefore it is of extreme importance to correctly model the fraction of the system which is superfluid.

The superfluid fraction is defined in terms of the dynamical response of the superfluid, which differs from the one of the normal component. For example, when a BEC is put in a rotating container, only the normal component reacts to this external perturbation and rotates along with the container; on the other hand, the superfluid remains still. So, the superfluid fraction may be defined as:

$$f = 1 - \frac{\langle L \rangle}{I_{cl}\omega},$$

where I_{cl} is the classical moment of inertia and ω the angular velocity of the container.

Let us now explain our approach to obtain the superfluid fraction. For conciseness, let us consider a two-dimensional box and a time-dependent potential moving with constant velocity along this box. As discussed previously for the rotating container, only the normal component reacts to the external perturbation and moves along with the potential. If we change to the reference frame in which the potential becomes time-independent, we see a static normal component while there appears a superfluid current in our system. By measuring the ground state's properties of this system we can obtain information about the superfluid current, in particular, the desired superfluid fraction.

The operator implementing the change of reference frame is the Galilean boost and it takes the form:

$$U = e^{i(\mathbf{v}\cdot\hat{\mathbf{P}}t + m\mathbf{v}\cdot\hat{\mathbf{R}})/\hbar}.$$

We are not interested in the actual translation of the system, but rather only in imprinting a relative velocity between the potential and the BEC. Therefore we can just set $t = 0$ and work with the following operator [1] :

$$U = e^{im\mathbf{v}\cdot\hat{\mathbf{R}}/\hbar}.$$

Applying this transformation to the GPE yields the following modified equation:

$$\frac{1}{2m}\left(\hat{\mathbf{P}} + m\mathbf{v}\right)^2 \phi(\mathbf{r}) + V(\mathbf{r})\phi(\mathbf{r}) + |\phi(\mathbf{r})|^2\phi(\mathbf{r}) = \mu\phi(\mathbf{r}), \tag{6}$$

where we see that we are just modifying appropriately the kinetic component of the equation by introducing a constant gauge. This change in the kinetic component yields an increase in the kinetic energy of the ground state of the modified equation when compared to the original GPE. The new ground state energy can be written as:

$$E(v) \approx E(0) + f\frac{mv^2}{2} \quad (v \to 0),$$

where in the second term there appears the kinetic energy associated with a current with velocity v [2]. More importantly, we have incorporated the fact that only the superfluid is flowing, and therefore it is the only component that contributes to the energy increase. This is the expression that we use to compute the superfluid fraction of our system:

$$f = \frac{E(v) - E(0)}{\frac{mv^2}{2}}.$$

Now let us discuss about the boundary conditions in the original and in the new reference frame. As it is usually done, in the reference frame in which the potential is static, we want to impose periodic boundary conditions. To derive the boundary conditions in the laboratory frame, let us consider the relation:

$$\phi(\mathbf{r}', t) = e^{im\mathbf{v}\cdot\mathbf{r}/\hbar}\psi(\mathbf{r}, t),$$

where ψ is the solution of the original GPE and ϕ that of the modified GPE. Taking into account that we are imposing periodic boundary conditions on ϕ, one finds that the corresponding boundary conditions for ψ are:

$$\psi(x = L, y, z) = e^{i\theta}\psi(x = 0, y, z),$$

where $\theta = mvL/\hbar$. This relation is called *twisted boundary condition*, and from the derivation, we see that this is completely equivalent to imposing a current in our system.

Now, we can either solve the modified equation with periodic boundary conditions, or the original GPE with the twisted boundary condition. Since the numerical scheme that we are using relies on the FFT algorithm, which requires the wavefunction to be periodic, we take the first approach.

[1] This new operator can be understood by considering the position operator as the generator of translations in momentum space.

[2] We must work in the limit $v \to 0$ to avoid generating excitations in the system.

2.2 Leggett's bounds

The study of the superfluid fraction of a system had a major breakthrough with the work of A. Leggett in Ref. [Leg70], that was later followed by a more detailed discussion in Ref. [Leg98]. In this last work, both an upper bound and a lower bound are given for the amount of superfluid fraction that we can find in a many-body system at T=0. In this section, we first present both bounds and then discuss the idea behind these expressions, and their conditions of applicability.

In his works, Leggett showed that given a bosonic dilute gas which sustains a current in the x-direction, a strict upper bound for its superfluid fraction is given by:

$$f^+ = \frac{1}{\bar{n}} \frac{1}{\left\langle \frac{1}{\langle n \rangle_{\{\xi\}}} \right\rangle_x}, \tag{7}$$

where $n = |\psi|^2$ is the particle number density (and $\bar{n} = N/V$ its mean value), $\langle ... \rangle_i$ represents the average over the i-th coordinate, and $\{\xi\}$ encompasses all degrees of freedom perpendicular to the axis where the current is applied. On the other hand, the lower bound for the superfluid fraction is given by:

$$f^- = \frac{1}{\bar{n}} \left\langle \frac{1}{\langle \frac{1}{n} \rangle_x} \right\rangle_{\{\xi\}}.$$

One important property of these bounds is that they reduce to the same expression in the cases of a *one-dimensional system*, or of a *separable density*:

$$f^- = f^+ = \frac{1}{\langle n_x \rangle \langle \frac{1}{n_x} \rangle}.$$

Since by definition $f^- \leq f \leq f^+$, in these two cases it is obvious that the superfluid fraction coincides with the value of the two bounds: $f = f^- = f^+$. To simplify the coming discussion, we will refer to this last identity as the "one-dimensional Leggett's result".

The upper bound is tightly connected to the existence of the so-called nodal surfaces, i.e., regions of space over which the density function vanishes. If we impose a current along the x-direction and the system hosts a y-slice with a vanishing density, then the upper bound becomes identically zero, because the superfluid cannot flow across that plane. The general statement would be to say that whenever we have a nodal surface perpendicular to the axis of the current, the superfluid fraction vanishes. How these nodal surfaces are generated completely determines the transition behaviour of the system, explaining, for example, the differences that we observe between 1D and 2D systems.

Let us now discuss the intuition behind these bounds. For simplicity, let us consider a two-dimensional box and a current in the x-direction, so that the two bounds take the simpler forms $f^+ = \left[\bar{n} \langle \frac{1}{\langle n \rangle_y} \rangle_x\right]^{-1}$ and $f^- = \frac{1}{\bar{n}} \left\langle \left[\langle \frac{1}{n} \rangle_x\right]^{-1} \right\rangle_y$.

We begin by considering the upper bound. Up to normalization factors, we first average over the y coordinate and then compute the one-dimensional Leggett's result using this effective transversal density. The key idea behind the upper bound is that, by first computing the y-average, we are erasing all information about the particular path the superfluid took to traverse the plane. Let us consider the toy example in the left panel of Fig. 1. The path we are showing there is highly improbable (i.e., energy-costly) since the entry and exit points are located far apart from each other. But, after averaging over the x_1 plane, we are just left with the total amount of superfluid that can cross that surface, independently of the particular region it crossed. Thus, since to measure the actual superfluid fraction the

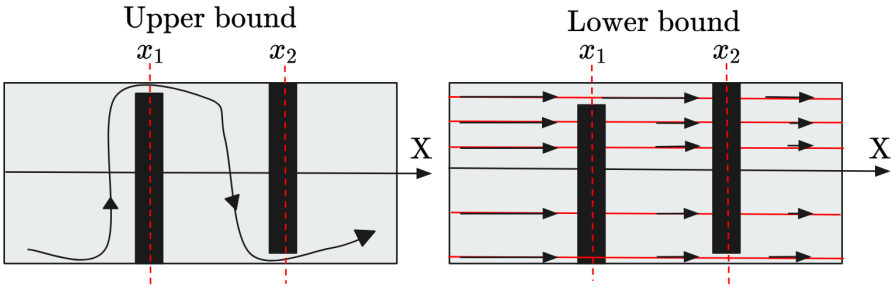

Figure 1: Toy model to understand how Leggett's upper and lower are generated. Black rectangles represent potential walls.

connectivity between the entry and exit point matters a lot, we are producing an upper bound.

To understand the idea behind the lower bound, we follow a similar approach. This time, instead of first considering y-slices of the system, we divide our system in one-dimensional tubes along the x-direction. We compute the one-dimensional Leggett's result along each one of these tubes, and then we average the results. By doing this, we are neglecting the fact that the superfluid cannot only tunnel through the potential barriers but can also flow around them. By ignoring the cross-talk between the tubes, we are effectively generating a lower bound for the superfluid fraction.

3 Superfluid fraction in an optical lattice

In this section, we study the response of the superfluid component to the presence of an optical lattice. As a first test of both the code and the bounds provided before, we reproduce the results presented in Ref. [CMR+23]. We studied first a 1D BEC in an optical lattice, and then a 2D BEC in presence of a 1D optical lattice [i.e., in both cases we take $V_{\text{ext}}(\mathbf{r}) = V_0[1 + \cos(2\pi x/a_{\text{latt}})]$, so that $\langle V \rangle = V_0$]. The latter is an example of a separable potential, which leads to a separable density. The behaviour is completely equal in both cases, according to the discussion presented before.

To translate the parameters used in Ref. [CMR+23] to our 1D and 2D setup, we first compute their chemical potential in units of the recoil energy $E_r = \frac{\hbar^2}{2m}\left(\frac{2\pi}{a_{\text{latt}}}\right)^2$. They used the following parameters:

$$n_0 = 60\,\mu\text{m}^{-2}, \qquad \frac{mg}{\hbar^2} = 0.15.$$

Then the chemical potential reads:

$$\mu_{2D} = n_0 g = 9\frac{\hbar^2}{m \cdot \mu\text{m}^2}.$$

Using the unit cell of the optical lattice (a_{latt}) as our length scale, and the recoil energy as the corresponding energy scale, the adimensional chemical potential reads:

$$\bar{\mu} = \frac{\mu}{E_r} = \frac{9\,\frac{\hbar^2}{m}\mu\text{m}^{-2}}{\frac{\hbar^2}{2m}\left(\frac{2\pi}{a_{\text{latt}}}\right)^2} = \frac{9}{2\pi^2}\frac{a_{\text{latt}}^2}{\mu\text{m}^2}.$$

They used an optical lattice whose constant is $a_{\text{latt}} = 3.93\,\mu\text{m}$, therefore:

$$\bar{\mu} = \frac{\mu}{E_r} = \frac{9}{2\pi^2} \cdot 3.93^2 = 7.042.$$

So, our effective one-dimensional and two-dimensional coupling constants, computed as $g_N = \mu/n_{0,N}$, are given by:

$$g_1 = \frac{\bar{\mu}}{n_{0,1}} = 7.042L, \qquad g_2 = \frac{\bar{\mu}}{n_{0,2}} = 7.042L^2,$$

where $n_{0,d} = 1/L^d$ and L is fixed by the grid used in the simulation.

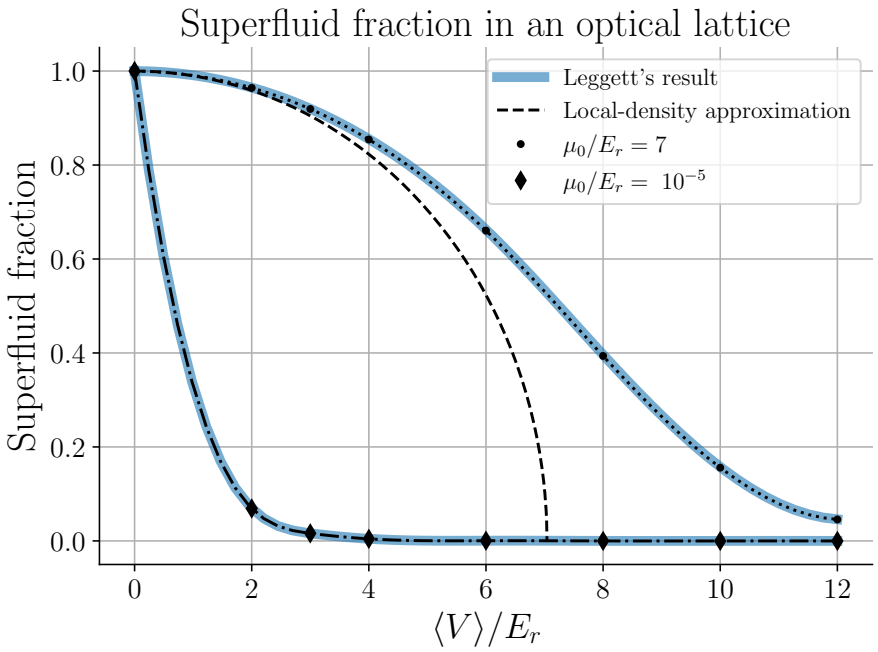

Figure 2: Superfluid fraction as a function of the depth of the optical lattice for two values of the mutual repulsion between bosons (i.e., of μ_0). The numerical datapoints are computed using twisted boundary conditions. Our results for a 1D system and a 2D system with a 1D optical lattice coincide and are identical to those found in Ref. [CMR+23].

Our numerical results for two different values of the chemical potential μ_0 are presented in Fig. 2. We present not only the results obtained through the method of the twisted boundary condition but also those computed using Leggett's result. We can clearly see that both quantities completely agree for all the values of g and amplitudes studied. Moreover, we have also verified numerically that the results of 1D and 2D systems are also completely equal, as expected for a separable density.

Analytically, the behavior of f may be understood in two different regimes:

- **Non-interacting regime**: for very weak interaction between the bosons (i.e., small μ_0), the system has no means to overcome the localization induced by the potential. This causes the superfluid fraction to rapidly disappear when the potential becomes noticeable, $1/f = \langle n \rangle \langle 1/n \rangle$ Ref. [CMR+23].

- **Local-density approximation (LDA)** : for strong repulsion and moderate optical potential, the kinetic energy becomes negligible, and the density takes the following (Thomas-Fermi) form: $n(\mathbf{r}) = [\mu - V(\mathbf{r})]/g$, with the restriction that $n(\mathbf{r}) \geq 0$. In this case, there is an analytical expression for the superfluid fraction [3]. When the

[3] $1/f = \langle n \rangle \langle 1/n \rangle = \mu/\beta \int_{-0.5}^{0.5} dx/[\mu/\beta - \cos(2\pi x)] = 2\mu/\left[\beta\pi\sqrt{(\mu/\beta)^2 - 1}\right] \lim_{x\to 1/2} \arctan\left[h\,(\mu/\beta)\tan(x\pi)\right] =$

potential becomes greater than the chemical potential, there appear extended regions in which the wavefunction vanishes. Thus the system cannot sustain currents, and the superfluid fraction goes to zero.

For general values of the optical lattice depth V_0 we see that f presents a smooth decay; the interplay between the repulsion of the particles and the optical lattice allows the system to sustain a superfluid component for deeper optical lattices.

4 Disordered potentials

In this work, we mainly want to study the behaviour of the superfluid fraction when the system is under the effect of a disordered potential. Let us briefly comment on why it is interesting to study the behaviour of quantum particles in this kind of potential. The vast majority of quantum systems that can be solved analytically are based on a series of assumptions that allow us to simplify them to a level where closed-form solutions can be found. Nonetheless, it is obvious that in a real quantum system, this idealistic situation can only be achieved to a certain degree, and some properties of the system, such as transport phenomena, can be heavily altered due to these small defects. One clear example of this situation, which is quite related to our work here, relates to the periodic structure in solids. For example, Bloch's theory is completely based on the fact that the potential felt by the particles is periodic. But it is well known that in real materials, this periodicity, when examined in shorter scales, shows certain irregularities that would destroy, totally or partially, the periodicity of the system. These spurious effects can be modelled using disordered potentials. The most prominent example of the effect of randomness in quantum systems is Anderson localization.

For us physicists, we can understand disordered potentials as smooth realizations of a random variable, for which we fix the mean value and the so-called correlation length. This last term is vital for understanding the physics of quantum systems in disordered potentials, as it gives the crucial length scale over which the effects of the disorder are noticeable.

In the following we introduce the kind of potential that we use, how it can be generated, and finally we characterize it.

4.1 Speckle potentials

Experimentally, a speckle pattern is generated by scattering light off a rough surface. Each independent scatterer emits new waves with a random phase producing the desired random pattern. A very good exploration of the topic can be found in Ref. [CVR+06].

Numerically we proceed in a very similar fashion. We define our simulation grid, and we choose an "aperture" in the middle of it. To each point of this aperture, we assign a random phase picked uniformly in the interval $[-\pi, \pi]$. Then, by computing the Fourier transform of this aperture function, we obtain the far-field approximation of the electric field and its modulus squared gives us the speckle pattern. An example of the potential we are using is shown in Fig. 3.

$\mu / \left[\beta\sqrt{(\mu/\beta)^2 - 1}\right]$.

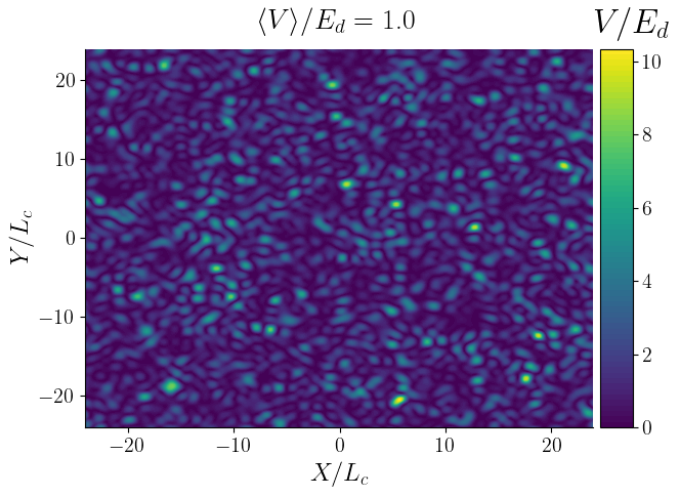

Figure 3: Realization of a two-dimensional speckle potential.

4.2 Statistical properties of the speckle potential

A relevant feature of our random potential is how the amplitude of the speckles is actually distributed. Since the scatterers are completely uncorrelated and the phases are random, the intensity distribution of a speckle pattern follows an exponential law:

$$P(V_i) = \frac{1}{\langle V\rangle} e^{-\frac{V_i}{\langle V\rangle}}.$$

From this, we can conclude that the standard deviation is determined by $\sigma = \langle V\rangle$. We must say that these results for the statistical properties of the potential only hold in the thermodynamic limit, for finite-size systems we should expect some deviations.

Another important parameter of our random potential is the average speckle size. To define it, we make use of the autocorrelation function. The two-point autocorrelation function is defined as:

$$C(\delta\mathbf{r}) = \langle V(\mathbf{r})V(\mathbf{r}+\delta\mathbf{r})\rangle.$$

We can compute this function by resorting to the Wiener-Khinchin theorem Ref. [Wei06], which states:

$$C(\delta\mathbf{r}) = \mathcal{F}^{-1}\left[\mathcal{F}\left[V(\mathbf{r})\right]\mathcal{F}\left[V(\mathbf{r})\right]^*\right],$$

where $\mathcal{F}$ and $\mathcal{F}^{-1}$ are, respectively, the Fourier transform and its inverse. Moreover, from the statistical properties of the potential, one can derive an analytical result for the autocorrelation function of the speckle potential in one dimension Ref. [Goo07]:

$$C(\delta x) = \langle V\rangle\left[1 + \mathrm{sinc}\left(\frac{\delta x}{L_c}\right)^2\right], \tag{8}$$

where $\mathrm{sinc}(x) = [\sin(\pi x)/(\pi x)]^2$ and L_c is the *correlation length*, which gives us the length scale over which the potential present correlated structures that we can understand as the speckles. The expression for higher dimensions is similar. This length scale allows us to define a characteristic energy scale for the disordered potential: $E_d = \frac{\hbar^2}{2mL_c^2}$.

In Fig. 4 we illustrate this statistical analysis for a specific realization of a one-dimensional speckle potential. We see that we have a very good agreement between the theoretical results and our numerical calculations, even for finite-size systems.

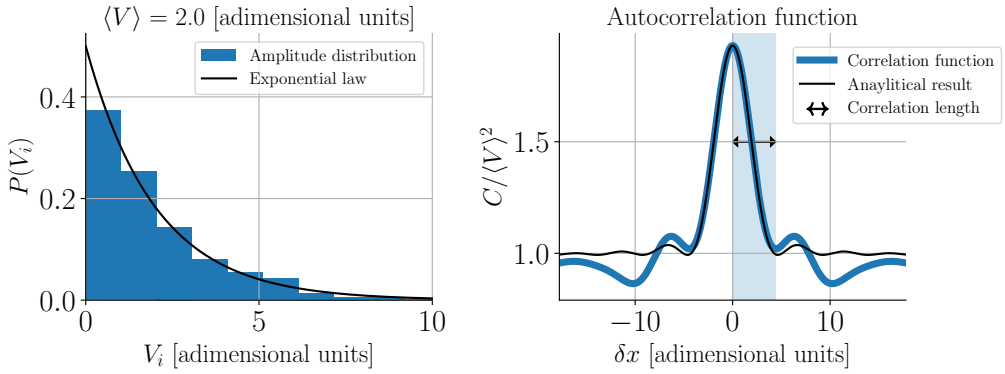

b

Figure 4: Left panel: the amplitude distribution of a speckle potential is well-fitted by an exponential law. Right panel: Autocorrelation function of the speckle potential and comparison with the analytical result Eq. (8). We are defining the correlation length by fitting the numerical result to a sinc function. Here we use a system size of $L = 150L_c$.

4.3 Self-averaging property

The random potential that we get from the above-described procedure obviously depends on the set of random numbers that we use each time for the phases. We are not interested in the properties of the BEC under the effect of a particular realization of the speckle potential, but instead, we want to obtain the general behaviour of a BEC under the effect of this class of random potentials. To achieve this, there are two paths that we can follow.

The first one consists in repeating our calculations for different realizations of the speckle potential for a fixed set of parameters, and averaging over the various outcomes.

On the other hand, if we are dealing with a system whose size is much larger than the average speckle size, the results obtained for a particular realization are already very close to the ensemble average. The basic idea behind this rapid convergence is that in the limit $L \gg L_c$ we can find (almost) every possible structure or combination of barriers that can be generated from the speckle so that the results obtained in the limit are basically the same as those obtained by explicit ensemble-averaging.

To test if this assumption is reasonable in our setups, we proceed as shown in Ref. [CVR+06]. In the infinite extent limit, the self-averaging property implies: $\sigma_{m_i}(\infty) = \langle m_i(\infty)^2\rangle - \langle m_i(\infty)\rangle^2 = 0$, where $m_i(d) = \frac{1}{d}\int_{-d/2}^{d/2}[V(x)]^i dx$ and the average is taken over different realizations of the disorder. If averaging over the disorder makes no difference, then our potential is indeed self-averaging. Using this criterion, we can put very specific conditions on when we are considering a potential to be self-averaging.

5 Superfluid fraction in a one-dimensional speckle potential

In this section, we present our results on the superfluid fraction in one-dimensional speckle potentials. Our main findings are shown in the right panel of Fig. 5.

First, we see that, as expected, our twisted boundary condition results completely agree with those computed using Leggett's result. Moreover, we have computed the transition curve for three different values of the coupling strength, finding that stronger interactions (smaller healing length) lead to superfluid currents that can be sustained against stronger disorder. Following this trend, we also observe that in this strong interaction regime, the transition from the conducting regime to the insulator one becomes much steeper. This

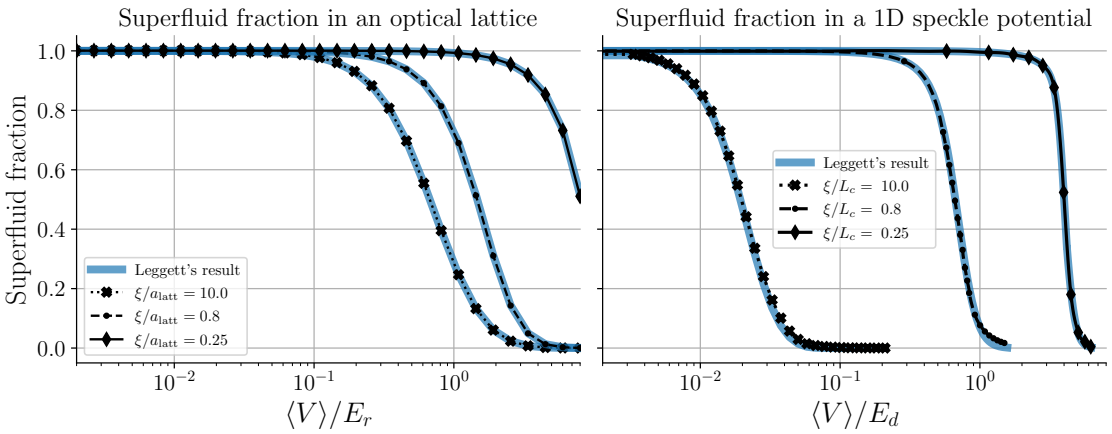

Figure 5: Left panel: Superfluid fraction of a BEC in an optical lattice as a function of the depth of the optical potential. Right panel: Superfluid fraction of a BEC in a 1D speckle potential as a function of the mean height of the speckles. The various curves are computed for different values of the boson-boson repulsion (quantified by the ratios $\xi/a_{\rm latt}$ and ξ/L_c, respectively). The "one-dimensional Leggett results" $[\langle\rho\rangle\langle 1/\rho\rangle]^{-1}$ are plotted as thick blue lines, and match perfectly the numerical data.

result is reasonable; the smaller the healing length, the easier the BEC can adapt to the potential, so to have a nodal surface, we need very high peaks, but once they appear the transition is immediate. On the other hand, when $\xi \gg L_c$ smaller peaks (that can be even spatially separated) are enough to generate regions with vanishing probability density, and these are generated more slowly.

Furthermore, it is interesting to analyze these results by comparing them with those for the optical lattice, which are shown in the left panel of Fig. 5. We observe that for similar system parameters, the transition takes place way earlier for speckle potentials, being this transition much steeper too. This result can be understood easily by analyzing the structure of the ground state in a speckle potential, Fig. 6. We see that even though most of the disorder peaks are relatively small, there are a few that have amplitudes notably larger than the average. As visible in the plot, in one dimension these few anomalously-high peaks alone can generate nodal surfaces in our density function. In one dimension, these nodal surfaces are nothing but extended regions over which the density vanishes. Then, we can easily understand why it is more difficult for the optical lattice to generate these nodal surfaces. We have to wait until its average value reaches a value comparable to that of the largest peaks of the speckle for it to be able to produce a vanishing density. The fact that all crests have the same amplitude is also responsible for the smoother transition observed for optical lattices. In this case, the nodal surfaces are steadily generated.

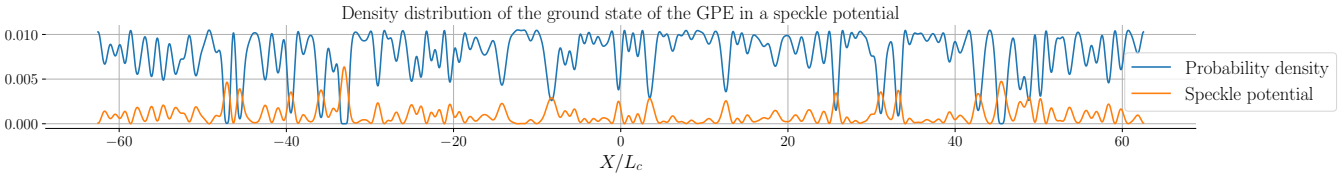

Figure 6: Ground state density of a BEC in a 1D speckle potential. This specific realization contains two "nodal surfaces", at around $x/L_c \approx -32$ and $x/L_c \approx 45$.

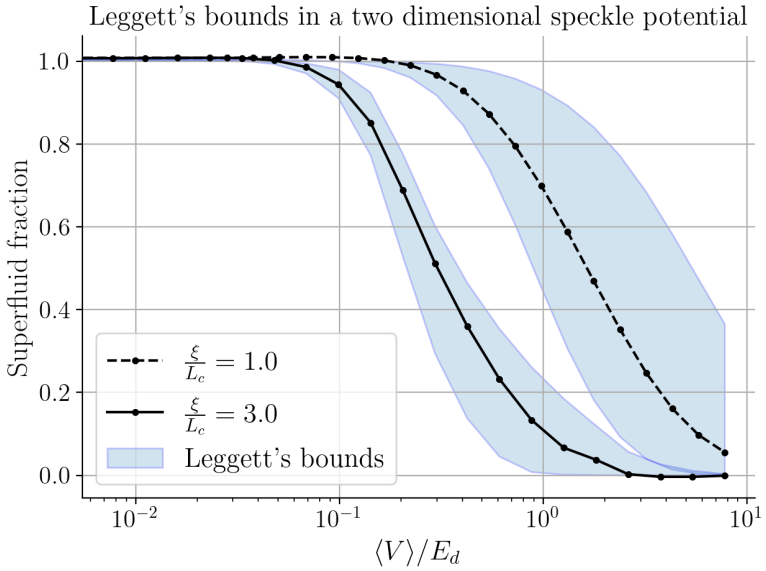

Figure 7: Superfluid fraction as a function of the average value of the speckle potential. The blue-shaded region represents the window provided by Leggett's bounds f^- and f^+. The right-most curve represents the behaviour of a BEC with stronger interactions.

6 Superfluid fraction in two-dimensional speckle potentials

In this section, we present the main results of our work, i.e., the analysis of the superfluid fraction in a 2D speckle potential. As opposed to the 1D optical lattice and speckle potentials, a 2D speckle pattern is a clear example of a non-factorizable potential. Because of this, the upper and lower bounds are no longer equal, so we can finally study how they behave as functions of the different parameters of the system. We first compute the superfluid fraction as a function of the average amplitude of the speckle, then discuss the appropriate choice of the wavefunction to compute the bounds. In addition, we analyze the generation of nodal surfaces in two-dimensional setups, comparing them to the one-dimensional case, and finally we discuss the finite-size effects present in our calculations, carefully extrapolating to the thermodynamic limit of infinite size.

The superfluid fraction f is presented in Fig. 7, along with the upper and lower bounds. Quite remarkably, these bounds provide a relatively narrow window for f; we see that the bracketing is looser in the transition region, but nonetheless, it still provides a small region for the superfluid fraction to be localized in. In particular, for this specific system we demonstrate that the bracketing is much tighter than the one estimated by Leggett himself, who expected the lower bound to be "likely much smaller than 1" Ref. [Leg98].

Moreover, we have plotted here the superfluid curve for two different values of the ratio ξ/L_c; we see that the weaker the coupling, the narrower the bracketing becomes. This is a result that we can easily intuitively understand. In the limit of a vanishing potential the density becomes "more separable", and, therefore, the upper and lower bounds approach the same value. On the other, in the limit of strong disorder the upper and lower bounds again converge to the same value since the upper bound collapses to zero by the generation of nodal surfaces in our density function.

So we have two limiting regimes (i.e. vanishing potential and strong disorder) in which upper and lower bounds coincide. For a weakly interacting Bose gas, the transition between these two regimes happens for smaller potentials and over a narrower interval when

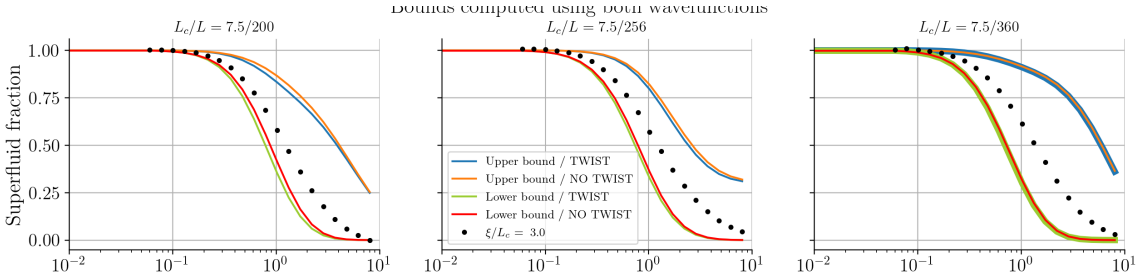

Figure 8: Leggett's bounds computed using both the twisted and untwisted wavefunction. From left to right, we are increasing the ratio L_c/L and we observe that the choice of the wavefunction becomes irrelevant.

compared to a strongly interacting gas. This is why we observe a tighter bracketing for weaker interactions.

We have not investigated the opposite limit of strong interactions further because the mean-field approach becomes increasingly worse there, but we do not expect the available window to grow up to a point where the bounds become useless. Rather, we expect to recover the kind of sharp transitions that we observed for a one-dimensional system. In this limit, the system can sustain the superfluid current up until a complete nodal surface appears. At this point, the superfluid fraction suddenly vanishes.

6.1 Choice of the wavefunction

Now, if we recall the procedure we are using to obtain the superfluid fraction, one can see that we are actually computing two different wavefunctions. So, which one do we have to use to obtain the bounds? In Fig. 8, we have plotted the behaviour of the bounds, computed using both wavefunctions, for three different system sizes (the system area is $L * L$). Our results show that the most stable bounds are found using the twisted wavefunction to compute the lower bound and the untwisted solution for the upper bound. More importantly, the difference seems to become irrelevant in the thermodynamic limit since the quantity θ/L approaches zero, and there is almost no difference between both solutions. Nonetheless, this choice is rather relevant for finite-size systems. Even though in Leggett's articles it is unclear which wavefunction should be used, our results are completely in-line with the discussion presented there.

6.2 Localization process in a two-dimensional speckle potential

Let us now further investigate the evolution of the probability density as the average value of the speckle amplitude increases. This is presented in Fig. 9. We see that relatively small potentials are again able to produce extended regions over which the probability density vanishes completely. Nonetheless, we do not see the sharp transitions that we had for its one-dimensional counterpart. This is because, as the dimensionality of the system increases, it becomes increasingly difficult for the potential to generate complete nodal surfaces (CNS). And this is precisely what we observe in our plot. A CNS in this setup corresponds to a y-slice over which the density function is zero (or very close to it); we see that due to the uncorrelated distribution of the speckles, we have to wait until the average value of our potential becomes very large, to be able to generate a disconnected probability density along the x-axis.

Taking a look at the density distribution, one can also understand the behaviour of the superfluid fraction as a function of the ratio ξ/L_c or, equivalently, as a function of

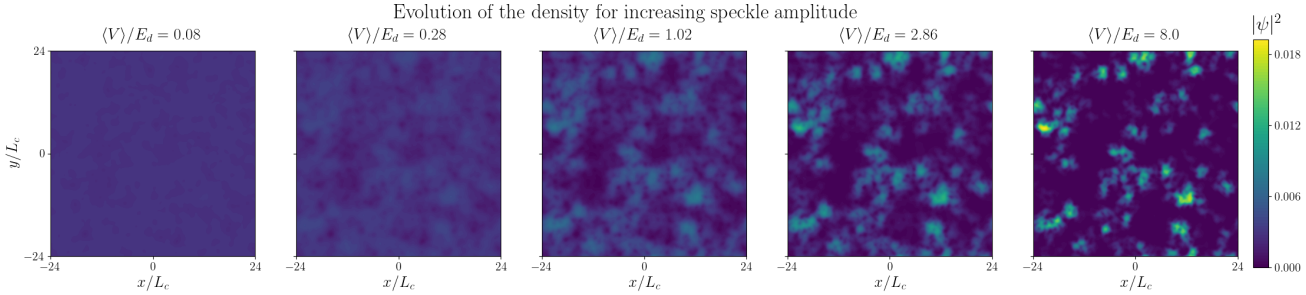

Figure 9: Localization process of a BEC in a two-dimensional speckle potential, for a bosonic gas with $\xi/L_c = 3.0$. From left to right we are increasing the average strength of the disorder. Here $|\psi|^2$ is normalized to one.

the coupling strength (see Fig. 7). If $\xi \gg L_c$ (i.e., for weak repulsion), the BEC is not able to prove the structure of the potential at all; therefore, it cannot find the wells of the potential. As a consequence, from the very moment that the mean amplitude of the speckles becomes noticeable (we have just seen that relatively small amplitudes are able to produce zeroes in the density), the BEC probability density has large regions over which it vanishes, prompting the appearance of the aforementioned nodal surfaces. In terms of the coupling strength (using a particle picture), the idea is the following; the particles display almost no resistance to be packed together, facilitating, therefore, the process of nodal surface generation, as there appear larger regions over which the density function vanishes.

To understand the opposite limit of strong repulsion, we proceed similarly. Now the BEC is able to detect and fill the deepest wells of the potential. These structures are completely uncorrelated due to the random nature of the potential, so it is reasonable to expect most y-slices to cross at least one of these wells. This limit can also be understood by considering that we are in the strongly interacting regime. Particles want to be as spread as possible, hindering the generation of nodal surfaces.

6.3 Finite size effects

In this section, we study how the superfluid fraction changes as we approach the thermodynamic limit. Since it is necessary to study systems that only encompass a couple of correlation lengths as well as those that are in the limit $L_c \gg L$, it is important to pay attention to the considerations presented in subsection 4.3. We have found that the superfluid fraction is reduced as the average size of the speckle and the size of the system grows. Our results are presented in Fig. 10, and are completely in-line with those presented in Ref. [AKN13], proving again that our approach and results are consistent and capable of reproducing known results[4]. Moreover, this is especially relevant because the authors of the latter work compared GPE results with exact ones obtained from diffusion Monte Carlo (DMC), giving further evidence of the validity of our conclusions.

From our results, it seems reasonable to propose a linear fit to retrieve the value in the thermodynamic limit of the form:

$$f(\infty) = f(L) + \frac{A}{L},$$

[4]Even though the overall behaviour is exactly the same, our curves for f as a function of $\langle V\rangle/E_d$ display a small offset with respect to the ones presented in Ref. [AKN13]. We have checked that we are able to reproduce exactly their results, when we used their potentials. Most probably, the origin of the offset is rooted in a slightly different way of computing the correlation length (which enters in the definition of E_d).

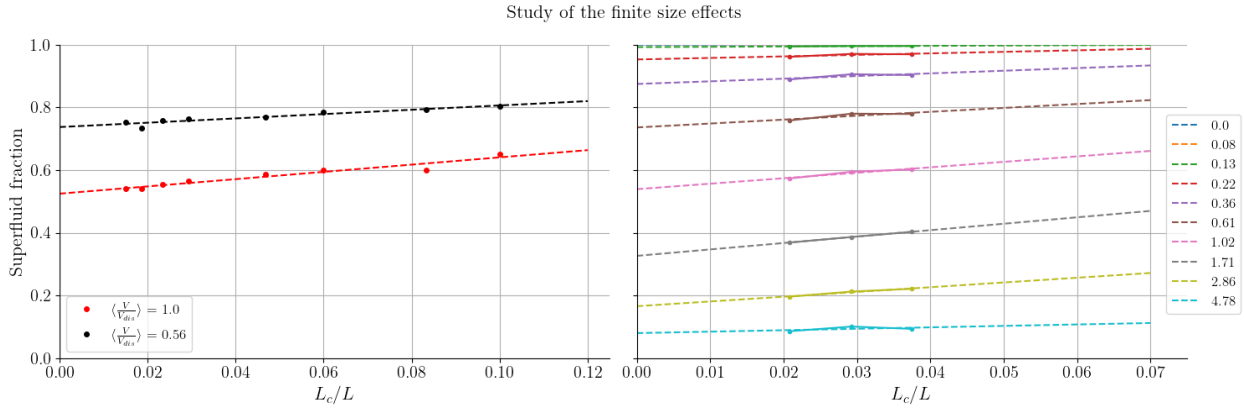

Figure 10: Relation between the superfluid fraction and the system size for $\xi/L_c = 3.0$. Points in both plots correspond to numerical calculation and the dashed lines are linear fits. In the right panel, the lines correspond, from top to bottom, to increasing values of the quantity $\langle V \rangle / E_d$. Note that the x ranges are not equal.

with $A < 0$. Another relevant comment that we can make about this plot is how the slope becomes steeper in the transition region while it remains notably flat in the two limiting regimes. This fact would allow us to obtain an estimate of the critical value of the potential that signals the transition between the conducting and the insulating regime.

7 Conclusions

In this last section, we summarize and put in context the results that we have presented in this work. First of all, we discussed and devised a scheme and a numerical method to retrieve the superfluid fraction of a system that can be well approximated by a mean-field description. We tested the validity of our approach by reproducing already published results, such as the recent Ref. [CMR+23] or those of Ref. [AKN13]. We also presented and discussed the results of A. Leggett on the upper and lower bounds to the superfluid fraction, providing the necessary intuition to understand their behaviour in different regimes.

Then, we presented a general discussion on the interest in studying disordered potentials, as well as providing an approach to generate and characterize the particular kind of potentials that we are using, the speckle patterns. Right after, we presented the results for a one-dimensional system. There we discussed the different behavior of the superfluid fraction in optical lattices and disordered potentials, explaining the key role that nodal surfaces play in the system's superfluid fraction. Moreover, we also provided numerical evidence of the validity of Leggett's result in different regimes.

In the last section, we presented novel results about the behaviour of the bounds for non-separable potentials. We begun by studying the applicability of the bounds, finding results that contradict Leggett's initial intuition. The available window provided by the bounds is relatively narrow, and the bracketing becomes even tighter as we approach the non-interacting regime. In addition to this, we also presented some intuition on how we can understand these results. To complete our comprehension of the bounds, we studied how to appropriately choose the wavefunction used to compute them. We also verified that, as expected, this choice becomes irrelevant in the thermodynamic limit. This analysis was followed by a discussion on the generation of nodal surfaces in two-dimensional systems. Comparing the results for a two-dimensional system with those of its one-dimensional counterpart, we provide an intuition of the role of dimensionality in the transition between

conducting and insulating states. We continued this discussion by analyzing the relation between the superfluid response and the coupling strength of the BEC.

We finally performed an analysis of the finite-size effects present in our system. We find that the superfluid fraction is reduced as we approach the thermodynamic limit and that this behaviour can be well approximated by a linear relation between the superfluid fraction and the inverse length.

8 Outlook

To conclude this work, we present some ideas that would be interesting to explore to further improve and complete our investigations of the topic. The first one, and probably the easiest as it has already been investigated, would be to complement our mean-field approach with Monte Carlo calculations, which would allow us to prove the limiting regime in which the GPE is no longer valid.

Another relevant topic that we would like to study is how the limits generalize to multicomponent systems. In his last article on the topic, Leggett provided some intuition on how one has to deal with this kind of systems and also on the difficulties that appear when doing so. We can understand multicomponent systems not only by considering different species of bosons (isotopes of the same boson, for example) but also by taking into account the internal degrees of freedom of the particles. For a two-species system, the GPE easily generalizes to a set of coupled equations, so we expect that a similar approach to the one we have used here can provide us with useful results. On the other hand, when taking into account internal degrees of freedom the dynamics of the system are heavily altered, for example, the number of particles of each species is no longer a conserved quantity. We probably need to go beyond the mean-field approach to correctly characterize our system, allowing us to study, for example, the tensor nature of the superfluid fraction since Hall-like effect may appear on the system.

On another route, it would be really interesting to study the behaviour of the bounds in fermionic systems. Again, Leggett discussed some of the complications that one faces in this case but also presented some hints on how to approach the task. The issue seems to be that a fermionic system may possess nodal surfaces (we have seen that they are crucial when studying superfluidity) that are completely dictated by symmetry considerations, while these do not appear in bosonic systems. How this new kind of structure may affect the superfluid behaviour of the system is not clear yet.

Finally, the approach to compute the bounds that we have described in our work seems to be relatively simple to reproduce experimentally. In Ref. [CMR+23], they found agreement between experimental results and Legett's result for separable densities. Exploring the bounds in a non-separable potential is more difficult but certainly worth exploring, especially after we have provided numerical evidence that the bounds provide a tight bracketing of the measured superfluid fraction. Moreover, even though in our work we have only studied a particular kind of disordered potential, it would be interesting to investigate whether there are significant changes for other types of random potentials, such as Bernoulli-disordered potentials. This line of research would allow us to study further how the bracketing varies in terms of the structure of the potential. We have seen that there are great variations when we go from a periodic to a non-periodic potential, so now changing the particular distribution of the peaks as well as their shape may also reveal interesting properties about the bounds.

A Numerical solution of the GPE

In this appendix we describe the numerical scheme used to solve the Gross-Pitaevskii equation. Even though we are tackling a time-independent problem, we make use of the time-dependent formula to obtain the ground state. The time-dependent equation can be derived by using the stationary action principle with a properly chosen lagrangian. It takes the following form:

$$-\frac{\hbar^2}{2m}\nabla^2\psi(\mathbf{r},t)+V(\mathbf{r})\psi(\mathbf{r},t)+g|\psi(\mathbf{r},t)|^2\psi(\mathbf{r},t)=i\hbar\frac{\partial\psi(\mathbf{r},t)}{\partial t}. \tag{9}$$

In this work, we use pseudo-spectral methods to solve for the ground state of the GPE. In particular, we employ both 2nd-order (Strang-Trotter splitting) and 4th-order (which are based on the latter) split-step Fourier methods combined with imaginary time evolution. In this section, we only provide a description of the algorithm; in Appendix B, a more detailed study on the accuracy and stability of the approach is presented.

Let us briefly summarize how these schemes work. According to Eq. (9), the condensate wavefunction evolves as:

$$\psi(\mathbf{r},t)=e^{-\frac{i\mu t}{\hbar}}\psi(\mathbf{r},0).$$

So we can identify the evolution operator of the system as:

$$\mathrm{U}(\mathbf{r},t)=\exp\left[-it\left(\frac{\mathbf{P}^2}{2m}+V(\mathbf{R})+g|\psi(\mathbf{x})|^2\right)\right]. \tag{10}$$

Therefore we obtain, at each time step, our evolved wavefunction by applying the following rule:

$$\psi(\mathbf{r},t+dt)=\mathrm{U}(\mathbf{r},dt)\psi(\mathbf{r},t).$$

The key insight of these pseudo-spectral methods is to notice that our time evolution operator has two different contributions, one that is diagonal in position representation and the other which is diagonal in momentum representation. Making use of the Zassenhaus formula (dual of the Baker-Campbell-Haussdorf formula) Ref. [Mag54] we can, to order $O(dt^2)$, approximate the evolution operator by:

$$\mathrm{U}(\mathbf{x},dt)\approx\exp\left[-i\,dt\frac{\mathbf{P}^2}{2m}\right]\exp\left[-i\,dt\left(V(\mathbf{R})+g|\psi(\mathbf{x})|^2\right)\right]+O(dt^2).$$

If we split the evaluation in the position representation into two parts, we can achieve an $O(dt^3)$ scheme called Strang splitting, Appendix B, that reads:

$$\mathrm{U}_2(\mathbf{r},dt)\approx\exp\left[-\frac{i\,dt}{2}\left(V(\mathbf{R})+g|\psi(\mathbf{r})|^2\right)\right]\exp\left[-i\,dt\frac{\mathbf{P}^2}{2m}\right]\exp\left[-\frac{i\,dt}{2}\left(V(\mathbf{R})+g|\psi(\mathbf{r})|^2\right)\right]+O(dt^3). \tag{11}$$

We can write this as follows:

$$\mathrm{U}_2(\mathbf{r},dt)=\mathrm{U}_{x/2}(\mathbf{r},dt)\,\mathrm{U}_\mathrm{K}\,\mathrm{U}_{x/2}(\mathbf{r},dt),$$

where the definition of the operators $\mathrm{U}_{x/2}$ and U_K is clear. Moreover, taking this splitting as a reference, we can even construct higher-order splittings by appropriately combining lower-order approximations. The following scheme, introduced by Suzuki Ref. [Suz91], offers an error of order $O(dt^5)$:

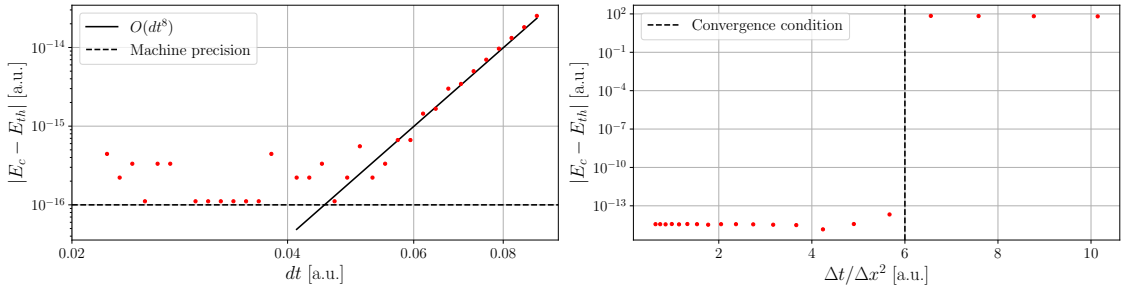

Figure 11: Right panel: Absolute error between the computed (E_c) and the theoretical (E_{th}) solution of a uniform initial guess in a two-dimensional harmonic potential, as a function of the time-step. Even though the method we provide is fourth-order accurate, due to the symmetries of harmonic Hamiltonian we are able to achieve an eight-order accuracy. Left panel: a similar study on the absolute error is performed against the ratio dt/dx^2, which is the relevant quantity in Von Neumann's stability analysis. We find that, as expected, our time and spatial step size must fulfil $dt < \alpha dx^2$ for some α of order unity. In this case, $\alpha \approx 6$. Here [a.u.] stands for dimensional units.

$$\mathrm{U}_4(\mathbf{r}, dt) = \mathrm{U}_2(\omega_0 dt)^2\, \mathrm{U}_2((1-4\omega_0)dt)\, \mathrm{U}_2(\omega_0 dt)^2,$$

with $\omega_0 = (4 - 4^{-1/3})^{-1}$. It is a characteristic of this kind of higher-order splitting formulas that one has to mix steps forward and backwards in time ($1 - 4\omega_0 < 0$). The novelty of the method proposed by Suzuki is that all prefactors ($\omega_0 dt, (1-4\omega_0)dt$) are kept smaller than unity, helping to maintain the method stable and accurate Ref. [McL93]. In exchange, we are forced to work with a six-stage method. A brief study on the accuracy and stability of the method is presented in Fig. 11

Once we have presented the fourth-order method that we employ in this work, the $O(dt^3)$ scheme update rule, which is used to construct the higher-order methods, goes as follows:

$$\psi(\mathbf{r}, t+dt) = \mathrm{U}_{x/2}\left[\mathcal{F}^{-1}\left[\mathrm{U_K}\,\mathcal{F}\left[\mathrm{U}_{x/2}\,\psi(\mathbf{r},t)\right]\right]\right],$$

where we have chosen the FFT algorithm to approximate the Fourier transform (and its inverse) and switch between position and momentum representation. Now there is only a subtlety that we must take into account to retain the third-order accuracy of the method. In the last step, we have already produced three different wavefunctions:

$$\psi_0 = \psi(t) \quad \psi_1 = U_{x/2}\psi_0 \quad \psi_2 = \mathcal{F}^{-1}\left[U_K \mathcal{F}[\psi_1]\right].$$

So which one should we use to construct the last evolution operator $U_{x/2}$? According to Ref. [JR06], in order to maintain the third-order accuracy of the scheme, we can use any linear combination $c_0\psi_0 + c_1\psi_1 + c_2\psi_2$ of the three wavefunctions as long as the coefficients satisfy: $c_2 = \pm 1$ and $c_1 = -c_0$. In particular, we take $c_1 = c_0 = 0$ and $c_2 = 1$, i.e., $\psi = \psi_2$.

A.1 Imaginary time evolution

We are interested in finding the ground state of our system. To achieve this, we use the imaginary time propagation method. It amounts to performing the change of variable $dt \to -id\tau$. It is easy to understand why this method allows us to project our initial guess onto the ground state. Let us consider that we are working with the Schrödinger equation, and we expand our initial guess $|\psi(0)\rangle$ in the energy eigenbasis $\{|e_i\rangle\}$:

$$|\psi(0)\rangle = \sum_i c_i(0)\,|e_i\rangle\,.$$

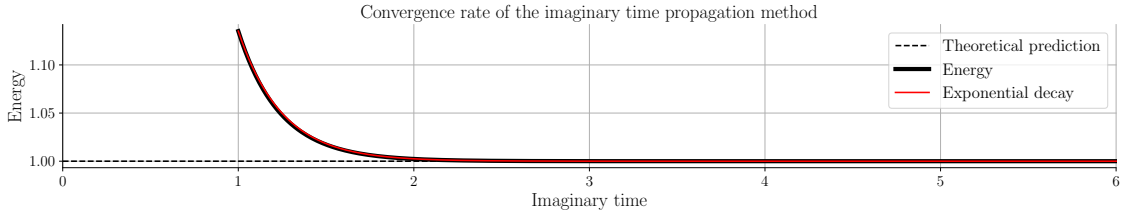

Figure 12: We present how the energy evolves as a function of the imaginary time for a uniform initial guess under the effect of a two-dimensional harmonic potential. We verify the convergence is, as expected, exponential.

Evolving this state, we obtain:

$$|\psi(t)\rangle = \sum_i c_i(0) e^{-i\frac{E_i}{\hbar}t} |e_i\rangle \,.$$

Now performing the change of variables to imaginary time, the resulting (unnormalized) state is:

$$|\psi(\tau)\rangle = \sum_i c_i(0) e^{-\frac{E_i}{\hbar}\tau} |e_i\rangle \,.$$

We see that as τ grows, we are suppressing exponentially fast the high energy components of the wavefunction, Fig. 12. If, after each iteration, we keep on normalizing our state, in the limit $\tau \to \infty$, we would get the ground state of the system. Here we see also that for τ finite, what we use, we may have problems identifying the first excited states from the ground state if their energies are too close. This is a huge issue for random potentials, where the gap can be quite small.

As a side note, this change of variable $dt \to -i\, d\tau$ is also known as a Wick rotation and can be understood as a kind of mapping between quantum mechanics and statistical mechanics. Therefore, in this new set of variables, what we are doing is cooling down the system to obtain the ground state.

One last final comment about this method is about its applicability to solve for the ground state of the Gross-Pitaevskii equation. Including the non-linearity in our evolution equation now cause the solutions not to be, necessarily, orthogonal. While this property of the solutions seems to be key in this method, one can show Ref. [Min18] that even if this set of orthogonal states is not guaranteed to exist, the imaginary time method still provides us with an energy-decreasing scheme that ultimately provides us with the ground state of the system.

B Strang splitting

We make use of the so-called Zassenhaus formula Ref. [Mag54] to split our evolution operator into several different terms. This formula is dual to the Baker-Campbell-Haussdorf expansion and is very useful for studying the splittings. To second order, it reads:

$$e^{k(A+B)} = e^{kA} e^{kB} e^{-\frac{k^2}{2}[A,B]} O(dt^3).$$

From here, it is trivial to identify $A = V + g|\psi|^2$, $B = \mathbf{P}^2/2m$ and $k = -i\, dt$ and arrive at a first-order expansion for the evolution operator:

$$U_1(\mathbf{r}, dt) \approx e^{-i\, dt(V+g|\psi|^2)} e^{-i\, dt\frac{\mathbf{P}^2}{2m}}.$$

We can, with almost no extra effort, produce a second-order expansion by writing the following:

$$U(\mathbf{r}, dt) = e^{-i\,dt(\frac{V+g|\psi|^2}{2}+\frac{\mathbf{P}^2}{2m}+\frac{V+g|\psi|^2}{2})},$$

and then, after a first use of the Zassenhaus formula:

$$U_2(\mathbf{r}, dt) \approx e^{\frac{-i\,dt}{2}(V+g|\psi|^2)}e^{-i\,dt(\frac{\mathbf{P}^2}{2m}+\frac{V+g|\psi|^2}{2})}e^{\frac{-dt^2}{4}\left[V+g|\psi|^2,\frac{\mathbf{P}^2}{2m}+\frac{V+g|\psi|^2}{2}\right]}+O(dt^3).$$

If now we expand again the middle term, we find:

$$U_2(\mathbf{r}, dt) \approx e^{\frac{-i\,dt}{2}(V+g|\psi|^2)}e^{-i\,dt\frac{\mathbf{P}^2}{2m}}e^{\frac{-i\,dt}{2}(V+g|\psi|^2)}e^{\frac{-dt^2}{4}\left[\frac{\mathbf{P}^2}{2m}+\frac{V+g|\psi|^2}{2},V+g|\psi|^2\right]}e^{\frac{-dt^2}{4}\left[V+g|\psi|^2,\frac{\mathbf{P}^2}{2m}+\frac{V+g|\psi|^2}{2}\right]}+O(dt^3),$$

so finally:

$$U_2(\mathbf{r}, dt) \approx e^{\frac{-i\,dt}{2}(V+g|\psi|^2)}e^{-i\,dt\frac{\mathbf{P}^2}{2m}}e^{\frac{-i\,dt}{2}(V+g|\psi|^2)}+O(dt^3).$$

Bibliography

[AKN13] G. E. Astrakharchik, K. V. Krutitsky, and P. Navez. Phase diagram of quasi-two-dimensional bosons in a laser-speckle potential. *Phys. Rev. A*, 87:061601, 2013.

[CMR+23] G. Chauveau, C. Maury, F. Rabec, C. Heintze, G. Brochier, S. Nascimbene, J. Dalibard, J. Beugnon, S. M. Roccuzzo, and S. Stringari. Superfluid fraction in an interacting spatially modulated bose-einstein condensate. *Phys. Rev. Lett.*, 130:226003, 2023.

[CVR+06] D. Clément, A. F. Varón, J. A. Retter, L. Sanchez-Palencia, A. Aspect, and P. Bouyer. Experimental study of the transport of coherent interacting matter-waves in a 1D random potential induced by laser speckle. *New Journal of Physics*, 8(8):165, 2006.

[Goo07] J. W. Goodman. *Speckle phenomena in optics: theory and applications*. Roberts and Company Publishers, 2007.

[JR06] J. Javanainen and J. Ruostekoski. Symbolic calculation in development of algorithms: split-step methods for the gross-pitaevskii equation. *Journal of Physics A, Mathematical and General*, 39(12):L179–L184, 2006.

[Leg70] A. J. Leggett. Can a solid be "superfluid"? *Phys. Rev. Lett.*, 25:1543–1546, 1970.

[Leg98] A. J. Leggett. On the superfluid fraction of an arbitrary many-body system at T=0. *Journal of Statistical Physics*, 93(3):927–941, 1998.

[Mag54] W. Magnus. On the exponential solution of differential equations for a linear operator. *Communications on pure and applied mathematics*, 7(4):649–673, 1954.

[McL93] R.I. McLachlan. Explicit symplectic splitting methods applied to PDEs. *Lectures in Applied Mathemathics*, 29:325–337, 1993.

[Min18] L. Mingarelli. *Simulating Infinite Vortex Lattices in Superfluids: A Novel Scheme and Its Applications*. Imperial College London, 2018.

[PS08] Ch. J. Pethick and H. Smith. *Bose–Einstein condensation in dilute gases*. Cambridge university press, 2008.

[Suz91] M. Suzuki. General theory of fractal path integrals with applications to many-body theories and statistical physics. *Journal of Mathematical Physics*, 32(2):400–407, 1991.

[Wei06] E. W. Weisstein. Wiener-Khinchin theorem. *From MathWorld–A Wolfram Web Resource*. http://mathworld.wolfram.com/Wiener-KhinchinTheorem.html, 2006.